Bandgap and doping effects in MoS$_2$ measured by Scanning Tunneling Microscopy and Spectroscopy

Chih-Pin Lu[1,2], Guohong Li[1] , Jinhai Mao[1], Li-Min Wang[2] and Eva Y. Andrei[1]

[1] Department of Physics and Astronomy, Rutgers University, Piscataway, New Jersey 08855, USA

[2] Department of Physics, National Taiwan University, Taipei 10617, Taiwan

Abstract

The discovery of graphene has put the spotlight on other layered materials including transition metal dichalcogenites (TMD) as building blocks for novel heterostructures assembled from stacked atomic layers. Molybdenum disulfide, MoS$_2$, a semiconductor in the TMD family, with its remarkable thermal and chemical stability and high mobility, has emerged as a promising candidate for post-silicon applications such as switching, photonics and flexible electronics. Since these rely on controlling the position of the Fermi energy (E_F) it is crucial to understand how it is affected by doping and gating. Here we employed scanning tunneling microscopy (STM) and spectroscopy (STS) with gating capabilities to measure the band gap and the position of E_F in MoS$_2$ and to track its evolution with gate voltage. For bulk samples the measured bandgap, ~1.3eV, is comparable to the value obtained by photoluminescence, and the position of E_F, 0.35eV below the conduction band, is consistent with n-doping reported in this material. Using topography together with spectroscopy we traced the source of the n-doping in bulk MoS$_2$ samples to point defects which we attribute to S vacancies. In contrast, for thin films deposited on SiO$_2$ we find significantly higher levels of n-doping which cannot be attributed to S vacancies. By combining gated STS with transport measurements in a field effect transistor (FET) configuration, we demonstrate that the source of the much higher n-doping in thin film samples originates with charge traps at the sample-substrate interface.

The development of techniques to isolate atomic layers[1] and to integrate them into atomically precise heterostructures[2] has enabled the design of novel material properties and applications by exploiting the proximity between layers with different electronic structures such as metallic (Graphene), insulating (hBN) and semiconducting (2H-MoS_2) [3-6]. 2H-MoS_2, a layered material in the transition metal dichalcogenite family has recently attracted much attention owing to its remarkable electrical and optical properties. The bulk has an indirect bandgap of 1.2~1.3 eV[7-10] which, due to quantum confinement, crosses over to a direct bandgap of ~1.9 eV when the material is exfoliated down to a monolayer[11] . Thin layers of MoS_2 are well suited as a channel material in FET applications exhibiting high room temperature mobility, almost ideal switching characteristics, and low standby power dissipation[6, 12-14]. Furthermore, the absence of dangling bonds and of surface states and its resistance to oxidation make MoS_2 a particularly good candidate for STM studies. In both bulk and thin layers of MoS_2 deposited on SiO_2 the conductivity consistently exhibits n-type character[6, 15-17] but to date source of the doping remains unclear. Proposals include substitutional impurities[14, 18] such as Cl, Br or Re[19], S vacancies[20-22], and impurities trapped at the interface with the SiO_2 substrate[3, 23]. Here we employ STM, STS combined with transport measurements to elucidate the nature of doping in MoS_2 and its connection to the switching characteristics of the thin layers.

Samples were prepared by exfoliating bulk *2H*-MoS_2 crystals (purchased from SPI) onto SiO_2 (300nm)/Si substrates to achieve the desired sample thickness and to expose a fresh sample surface. MoS_2 flakes were identified by optical microscopy and subsequently characterized by atomic force microscopy (AFM), Raman spectroscopy and photoluminescence in ambient conditions. The AFM height profile of one of the samples, shown in Fig.1(a), indicates a thickness of 4.2 nm corresponding to 6 layers. The Raman spectra, Fig.1(b), for single, multilayer and bulk MoS_2 samples show a

monotonic evolution with the number of layers [24]. For the 6-layer sample the spectrum is already very close to that of bulk. FET devices were fabricated using e-beam lithography with Ti/Au (2 nm/60 nm) contacts deposited by electron-beam evaporation at a base pressure of 2×10^{-7} Torr. Prior to measurements the MoS_2 devices were baked for 3hrs in forming gas (90% Ar, 10% H_2) at 230 ^{0}C. STM and STS measurements were performed at 80 K in a home-built STM[25-28] using mechanically cut Pt-Ir wire tips. The topographic STM images were recorded in constant current mode with the bias voltage, V_b, applied to the sample while the STM tip was held at ground potential. The differential conductance spectra, dI/dV, were measured using lock-in detection (f = 440Hz) with fixed tip to sample distance. Gated STS measurements were carried out in a device configuration, shown in Fig.1(c), in which a thin sample was deposited on a 300nm SiO_2 substrate capping a degenerately p-doped Si gate.

To investigate the source of doping in thin MoS_2 samples we employed a 6 layer sample configured in an FET device which combines STS with gating capability. As shown in the STM topography image in Fig.2(a) the sample surface is relatively flat and clean with corrugations not exceeding ~ 0.2nm over a 50nm × 50nm area. Zooming in to atomic resolution in Fig.2(b) reveals the Sulfur surface atoms arranged in a triangular lattice with lattice constant ~ 0.31 nm, in agreement with the accepted crystallographic value, of 0.316 nm. This indicates high surface quality with no surface contamination left over from the fabrication process. STS measurements at the same position revealed a bandgap of ~ 1.2 ± 0.1 eV which comparable to the reported photoluminescence gap[10] suggesting that tip induced band-bending does not significantly affect our measurements . Using the setup shown in Fig.2(c) we studied the local electronic properties as a function of doping by applying a gate voltage, V_g, across the SiO_2 substrate. For $V_g = 0$V we find that E_F is at the edge of the conduction band (CB) indicating the presence of shallow donors, in agreement with previous

reports of unintentional n-doping of such devices[3, 6]. Furthermore, applying $V_g = -25$V

shifts the position of E_F to the center of the bandgap, as shown in Fig.2(c). Following

the evolution of the spectra with V_g, we find that E_F rapidly moves from the center of

the bandgap towards the CB as V_g becomes more positive, and reaches it at a threshold

voltage, $V_{gt} \sim -15V$, as shown in Fig.2(d).   Once E_F enters the CB its evolution with

V_g slows down significantly reflecting the higher density of states within the band.

From the evolution of E_F with V_g in the gap region, inset in Fig.2(d),   we obtain

$dE_F/dV_g = 0.06q$, where q is the magnitude of the electron charge. Rewriting this

expression in terms of the quantum capacitance[29], $C_Q = q^2 \dfrac{dn}{dE_F}$, where n is the

carrier density per unit area, we obtain $\dfrac{dE_F}{dV_g} = \dfrac{1}{q}\dfrac{dE_F}{dn}\dfrac{dqn}{dV_g} = q\dfrac{C}{C_Q}$. Noting that

$\dfrac{dqn}{dV_g} = C = (1/C_{ox} + 1/C_Q)^{-1}$ is the total device capacitance resulting from the series

connection of C_Q with the oxide capacitance, $C_{ox} = \varepsilon_{ox}/d_{ox} \approx 12nF \cdot cm^{-2}$, and

rewriting $\dfrac{dE_F}{dV_g} = 0.06q = q\dfrac{C}{C_Q}$,   we find $C_Q/C_{ox} = 15.6nF \cdot cm^{-2}$. This gives

$C_Q = 187nF \cdot cm^{-2}$, $C = 11.3nF \cdot cm^{-2}$ for our device. From the quantum

capacitance we can obtain the total density of states per unit area: $\dfrac{dn}{dE_F} \equiv \mathcal{D}(E_F) \sim 1.16$

$\times 10^{12}$ states/eVcm^2.   Furthermore, using the measured threshold voltage, $V_{gt} = -15$V,

and the value of C we can estimate the initial carrier density in the ungated sample: n_0

$= CV_{gt}/q \sim 10^{12}$cm^{-2}. We next compare the STS results to transport measurements of

a thin sample in an FET device configuration.

In order to correlate the STS data with transport measurements we used a 2-

terminal device configuration shown in Fig.3 to follow the gate dependence of the drain

source current, $I_{ds}(V_g)$ in 4 samples (Supplementary material). We found that the device

characteristics such as mobility and subthreshold slope improve substantially after in-

situ annealing in vacuum (10^{-6} mbar) at 120 ^{0}C for 20 hours, similar to results reported in the literature[3]. For the 2 layer sample shown in Fig.3(b), the conduction threshold, initially $V_{gt} = 8$V, decreased after annealing to $V_{gt} = -10$V approaching the value obtained by STS. From the measured gate dependence we obtain the field-effect mobility at 300K $\mu = \dfrac{L}{WC_{ox}} \dfrac{1}{V_{ds}} \dfrac{dI_{ds}}{dV_g}$ ~3cm^2 V^{-1} s^{-1} which increased to ~6 cm^2 V^{-1} s^{-1} after annealing. Here L = 7.4 µm, W = 6.5 µm are the channel length and width respectively. Another important metric of device quality is the subthreshold swing[30] defined as $S = (ln10)k_BT/q$ (1+C_Q/C_{ox}). The subthreshold swing, which can also be expressed as $S = \dfrac{dV_g}{d(log\,I_{ds})}$, characterizes the switching time of the device: the lower S the faster the device. Its value can be obtained from I_{ds} (V_g), by measuring the subthreshold slope: $\dfrac{d(log\,I_{ds})}{dV_g}$. For $C_Q \ll C_{ox}$ the device reaches its thermodynamically limited fastest performance with $S_{min} = (ln10)k_BT/q$ =60mV/decade at T = 300K. This is significantly below the S values measured in our devices indicating that they operate in the opposite limit $C_Q \gg C_{ox}$. For the sample discussed here, S=1.5V/decade at T=300K prior to annealing, gives an estimated C_Q ~288nF cm^{-2} $\gg C_{ox}$. The device improved after annealing dropping to S = 0.7V/decade, and C_Q ~128nF cm^{-2}. Remarkably, the values of C_Q obtained by transport agree with the STS values within the experimental uncertainty indicating that transport measurements can provide a reliable measure of the quantum capacitance.

The change in sample quality after annealing (supplementary material) and the weak dependence of S on sample thickness suggest that surface traps significantly contribute to the doping observed in these devices. In order to trace the origin of the doping and to establish whether it is due to bulk or surface traps, we carried out STM/STS on a freshly cleaved bulk sample whose surface has not undergone wet treatment and that is not supported by an SiO$_2$ substrate. The sample was mounted into

the STM head using silver paint to attach the back of the sample to a reference electrode. STS measurements on the bulk sample reveal a band gap of ~ 1.3 eV, Fig.4(c), consistent with the photoluminescence results. Contrary to the results in the thin sample, E_F is now ~ 0.35 eV below the CB indicating the presence of deep donors. Indeed large area (50 nm×50 nm) STM topography , shown in Fig. 4(a,b), which was obtained at V_b = 1.2V reveals defects as dark spots. Three types of defects can be distinguished by their apparent depth and diameter: darkest −0.12 nm, 3 nm diameter; intermediate −0.05 nm deep, 4 nm diameter; faint −0.02 nm deep 5.5 nm diameter. Zooming into the defects to resolve the atomic structure we find that the lattice periodicity is intact suggesting that the defects are buried under the surface. According to *ab* initio calculations the electronic structure of point defects on the surface of MoS_2 are tightly localized within one atomic distance[19]. By contrast, the defects observed here are extended several lattice spacings with no signature of a localized feature on the central atom. This again indicates defects buried under the surface, similar to the case of buried Mn impurities in GaAs or InAs which produce a topography signature extending over several lattice spacing[31-33]. Amongst the reported substitution atoms in MoS_2, only Cl, Br and Re are consistent with n-doping. However the ionization energy of these donors, ~0.16 eV, 0.26 eV and 0.06 eV respectively[18, 19] , is too low to account for the observed E_F ~ 0.35 eV below the CB. Furthermore, X-Ray Fluorescence (XRF) and X-ray photoelectron spectroscopy (XPS) analysis of our crystal indicated that within the experimental resolution of 100 ppm these elements were not present. As we show next the observed defects are consistent with S vacancies.

Zooming into the center of a defect, Fig. 4(d), the STS spectra reveal a sharp in-gap peak at V_b = −0.94V which is close the valence band and not near the CB edge where donor states are expected. This apparent discrepancy reflects the tip-induced band bending[34]. When the bias voltage corresponds to the flat band condition the donor

state crosses E_F creating a new conduction path where donor electrons tunnel into empty states of the STM tip which gives rise to a peak in the differential conductance. We can calculate the donor ionization energy, E_d, from the flat band condition: $qV_{FB} = E_A + \frac{E_d}{2} - \Phi_{tip}$, where $V_{FB} = -0.94$ eV the flat-band bias voltage, E_A=4.2 eV the electron affinity in MoS_2[35, 36], and Φ_{tip} the work function of the tip. Using the value[37] $\Phi_{tip} = 5.5$eV for the Pt-Ir tip we obtain $E_d \sim 0.7$ eV below the CB consistent with the position of E_F and with the calculated values for S vacancies[18-22]. This gives an estimate of the defect size[32]: $R \sim \frac{\hbar}{\sqrt{2m^*E_d}} = 0.3nm$ (m* =0.4m_e is the effective electron mass) which agrees with the calculated size of an S vacancy[19]. However, when buried under the surface point defects produce a more extended topography image which typically increases with the depth[31-33] consistent with the fact that the atomic topography image shows no missing surface atoms, Fig. 4(b). The three defect sizes can be understood in terms of vacancies located in different S layers underneath the surface [32, 33]. To estimate the density of vacancies we measure the surface density of defects of equal size, $N_l \approx 3.5 \times 10^{10} cm^{-2}$ and assuming the same defect density in all S layers we obtain the volume density: $N_{3d} = N_l / a \approx 1.1 \times 10^{18} cm^{-3}$ where $a = 0.31$ nm is the vertical separation between   sulfur layers. At room temperature this gives an activated bulk carrier density of $n \sim N_{3d} e^{-(E_F - E_D)/k_B T} \approx 10^{13} cm^{-3}$ in the ungated devices. We can now estimate the equivalent areal density of activated carriers in the double layer, t ~ 2.5 nm, used in the FET device above to be $n_0 = nt \sim 2.5 \times 10^4 cm^{-2}$, which is significantly lower than the measured residual density in thin devices. These results clearly exclude bulk mechanisms such as substitutional dopants or sulfur vacancies, as the source of the post-anneal doping observed in thin layer MoS_2. We must conclude that the n-doping in the thin layer is due to trapped charges at the interface with the SiO_2 substrate,

consistent with the observed variability in device quality and with the post-anneal improved performance[3, 23]. Likely candidates for the trapped charges could be Na ions which are notoriously prone to contaminate[38] the surface of SiO_2. For example in the case of graphene deposited on SiO_2 it is well known that trapped Na ions at the interface cause significant levels of unintentional doping, however there Na produces holes whereas in MoS_2 it induces electron doping[23, 39].

In summary by combining STM, STS and gating capabilities together with transport measurements we have traced the origin of the intrinsic n-doping in bulk 2H-MoS_2 to S vacancies. Within the experimental error we found no evidence of Cl, Br, or Re dopants. Furthermore, we demonstrated that the source of the significantly higher n-doping observed in thin films deposited on SiO_2 is extrinsic and can be attributed to trapped donors at the interface with the SiO_2 substrate.
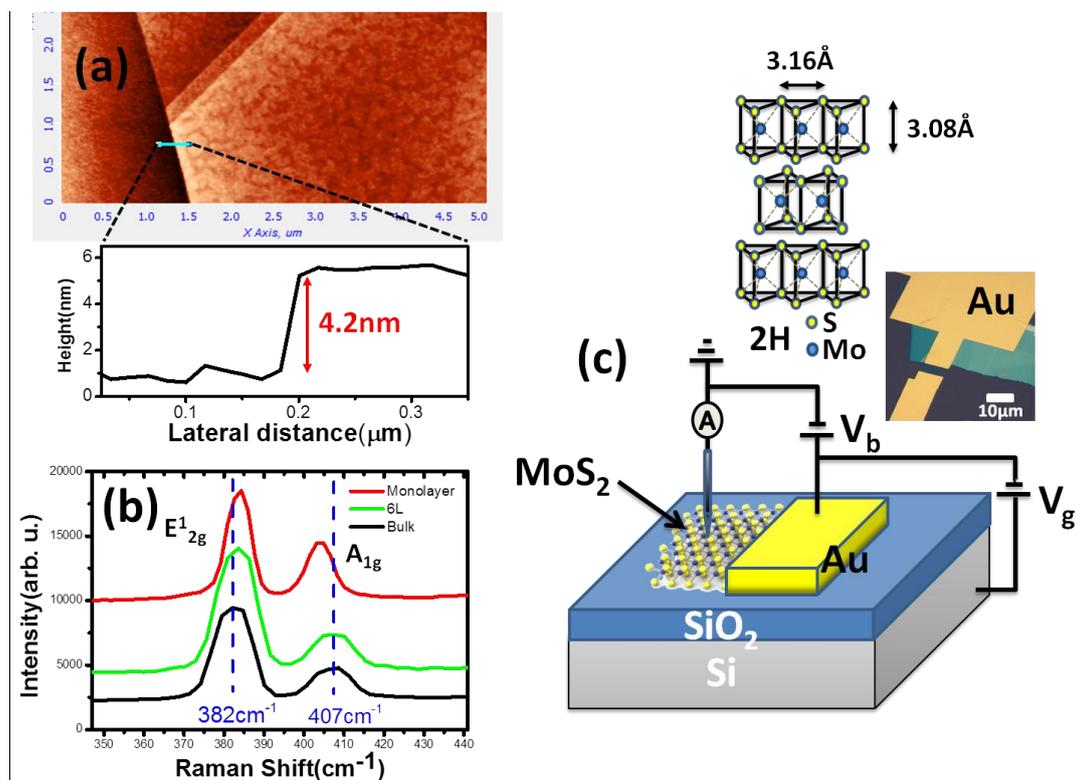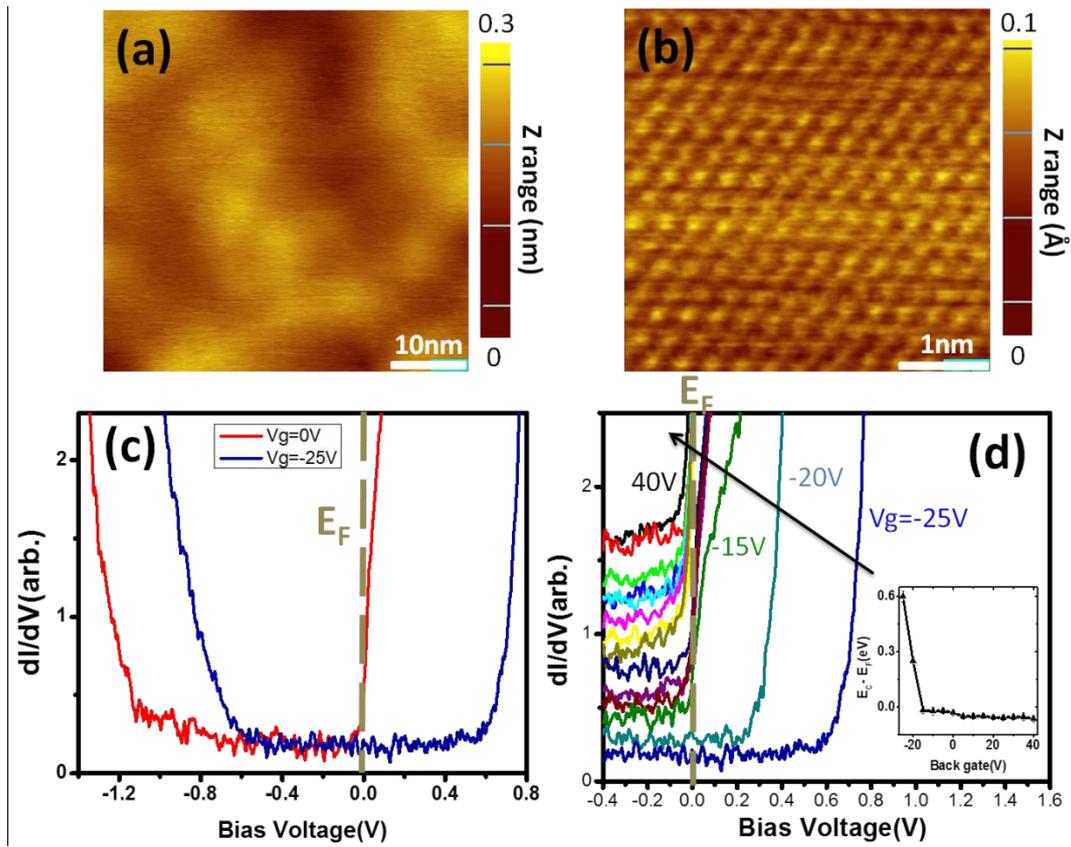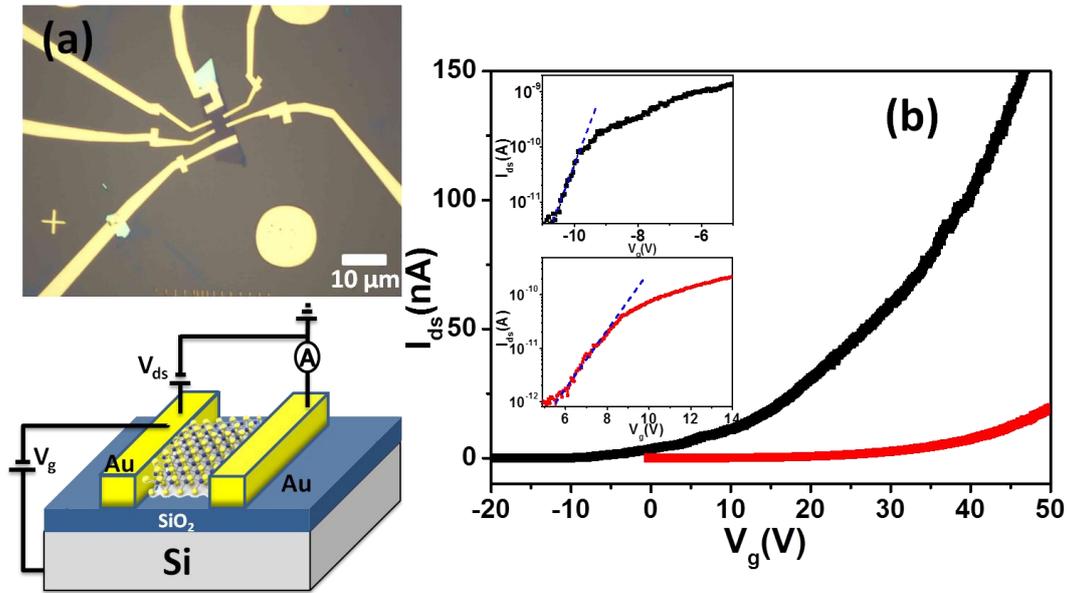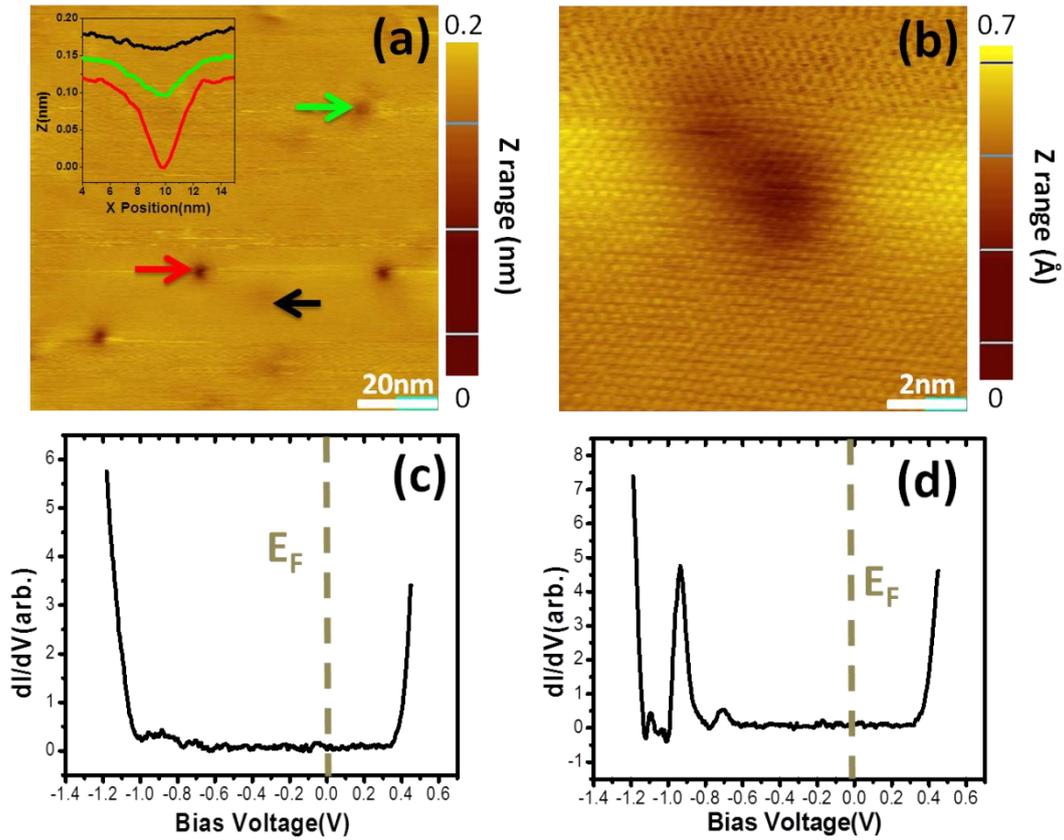
FIGURES:

Figure 1. (a) AFM image of multilayer MoS_2 on a SiO_2/Si substrate. The step height indicates a thickness of 4.2nm corresponding to 6 layers. (b) Raman spectrum showing the in-plane E^1_{2g} and out-of-plane A_{1g} resonances of single, multilayer and bulk MoS_2. The laser wavelength was 633 nm and the spot size ~2 μm. (c) Schematic of MoS_2 sample mounted in an STM configuration with gating capabilities. The sample bias V_b is applied between the STM tip and the MoS_2 sample contacted by a Ti/Au electrode. The back gate voltage V_g is applied between the p-doped Si substrate and the top electrode. Inset: Optical micrograph of a mechanically exfoliated multilayer MoS_2 flake and schematics of the atomic structure of 2H-MoS_2.

Figure 2. (a) STM constant current topography image of a 6 layer MoS_2 sample measured in the device configuration of Fig. 1(c) for $V_b = 1.4$ V and I = 20 pA. (b) Same as (a) zooming in to atomic resolution. (c) dI/dV spectrum taken in the area shown in (b) for $V_g = 0$V (red) and $V_g = -25$V (blue) (d) Evolution of dI/dV spectrum with V_g. Curves are offset vertically and only show the CB edge. Inset: Gate voltage dependence of the position of the Fermi energy relative to the bottom of the conduction band.

Figure 3. (a) Top: Optical micrograph of a thin MoS_2 device supported on a 300nm-thick SiO_2 substrate configured for a 2-terminal transport measurements. Bottom: Schematic of the MoS_2 FET device. (b) Evolution of source-drain current, I_{ds}, with V_g at 300K and $V_{ds} = 0.1V$ for the device shown in (a). The red and black curves correspond to measurements before and after annealing respectively. Inset: same data on a semi-logarithmic scale.

Figure 4. (a) STM constant current topography image of a 50nm × 50nm area at V_b = 1.4V and I = 20 pA on bulk MoS_2 showing 3 types of defects with different apparent depths as indicated by the height profiles in the inset. (b) Constant current STM atomic resolution image on one of the defects. (V_b = 1.2 V and I = 20 pA). (c) dI/dV spectrum taken far from any defect. (d) dI/dV spectrum taken on the defect shows a pronounced in-gap resonance near −0.94 V. The Fermi level is ~ 0.35 eV below the CB edge. The measurement was referenced to a set-point with tunneling resistance 15 GΩ (bias voltage V_b =1.5V and tunneling current I =100 pA).

RERERENCES

1.   Novoselov, K. S.; Jiang, D.; Schedin, F.; Booth, T. J.; Khotkevich, V. V.; Morozov, S. V.; Geim, A. K. *PNAS* **2005,** 102, 10451.

2.   Geim, A. K.; Grigorieva, I. V. *Nature* **2013,** 499, (7459), 419-425.

3.   Ayari, A.; Cobas, E.; Ogundadegbe, O.; Fuhrer, M. S. *Journal of Applied Physics* **2007,** 101, (1), 014507.

4.   Wang, Q. H.; Kalantar-Zadeh, K.; Kis, A.; Coleman, J. N.; Strano, M. S. *Nature nanotechnology* **2012,** 7 699-712.

5.   Chhowalla, M.; Shin, H. S.; Eda, G.; Li, L.-J.; Loh, K. P.; Zhang, H. *Nature Chemistry* **2013,** 5, 263-275.

6.   Radisavljevic, B.; Radenovic, A.; Brivio, J.; Giacometti, V.; Kis, A. *Nature nanotechnology* **2011,** 6, 147-150.

7.   Kam, K. K.; Parkinson, B. A. *J. Phys. Chem.* **1982,** 86, 463-467.

8.   W.K. Ho, J. C.Yu, J. Lin, J. G.Yu,   P. S.Li. *Langmuir* **2004,** 20, 5865.

9.   E. Gourmelon, O. Lignier,H. Hadouda, G. Couturier, J. C. Bernede,J. Tedd, J. Pouzed and J.   Salardenne. *Sol. Energy Mater. Sol. Cells* **1997,** 46, 115.

10. Mak, K. F.; Shan, J.; Heinz, T. F. *Physical Review Letters* **2010,** 104, (17), 176404.

11. Andrea Splendiani, Liang Sun, Yuanbo Zhang, Tianshu Li, Jonghwan Kim, Chi-Yung Chim, Giulia Galli and Feng Wang. *Nano Lett.* **2010,** 10, 1271-1275.

12. Han Wang, Lili Yu, Yi-Hsien Lee, Yumeng Shi, Allen Hsu, Matthew L. Chin, Lain-Jong Li, Madan Dubey, Jing Kong, Tomas Palacios *Nano letters* **2012,** 12 4674-4680.

13. Hai Li, Zongyou Yin, Qiyuan He, Hong Li, Xiao Huang, Gang Lu, Derrick Wen Hui Fam, Alfred Iing Yoong Tok, Qing Zhang, and Hua Zhang. *Small* **2012,** 8 63-67.

14. Zongyou Yin, Hai Li, Hong Li, Lin Jiang, Yumeng Shi, Yinghui Sun, Gang Lu, Qing Zhang, Xiaodong Chen, and Hua Zhang *ACS Nano* **2012,** 1, 74-80.

15. Radisavljevic, B.; Kis, A. *Nature nanotechnology* **2013,** 12, 815-820.

16. Sunkook Kim, Aniruddha Konar,Wan-Sik Hwang,Jong Hak Lee,Jiyoul Lee,Jaehyun Yang,Changhoon Jung,Hyoungsub Kim,Ji-Beom Yoo,Jae-Young Choi,Yong Wan Jin,Sang Yoon Lee,Debdeep Jena,Woong Choi and Kinam Kim. *Nature Communications* **2012,** 3, 1011.

17. Britton W. H., Baugher, Hugh O. H. Churchill, Yafang Yang, and Pablo Jarillo-Herrero *Nano Lett.* **2013,** 13, 4212-4216.

18. Carvalho, A.; Neto, A. H. C. *Physical Review B* **2014,** 89, (8), 081406.

19. Noh, J.-Y.; Park, M.; Kim, Y.-S.; Kim, H. *arXiv:1307.3813* **2013**.

20. Fuhr, J. D.; Saul, A.; Sofo, J. O. *Phys. Rev. Lett.* **2004,** 92, 026802.

21.   Kim, B. H.; Park, M.; Lee, M.; Baek, S. J.; Jeong, H. Y.; Choi, M.; Chang, S. J.; Hong, W. G.; Kim, T. K.; Moon, H. R.; Park, Y. W.; Park, N.; Jun, Y. *RSC Advances* **2013,** 3, (40), 18424-18429.

22.   Qiu, H.; Xu, T.; Wang, Z.; Ren, W.; Nan, H.; Ni, Z.; Chen, Q.; Yuan, S.; Miao, F.; Song, F.; Long, G.; Shi, Y.; Sun, L.; Wang, J.; Wang, X. *Nat Commun* **2013,** 4.

23.   Dolui, K.; Rungger, I.; Sanvito, S. *Physical Review B* **2013,** 87 165402.

24.   Changgu Lee, Hugen Yan, Louis E. Brus, Tony F. Heinz, James Hone, and Sunmin Ryu *ACS Nano* **2010,** 4 2695-2700.

25.   Li, G.; Andrei, E. Y. *Nat. Phys.* **2007,** 3, (9), 623-627.

26.   Luican, A.; Li, G.; Andrei, E. Y. *Solid State Communications* **2009,** 149, (27-28), 1151-1156.

27.   Andrei, E. Y.; Li, G.; Du, X. *Reports on Progress in Physics* **2012,** 75 056501

28.   Li, G.; Luican, A.; Andrei, E. Y. *The Review of scientific instruments* **2011,** 82, (7), 073701.

29.   Luryi, S. *Appl.Phys.Lett.* **988,** 52, (6), 501-503

30.   Sze, S. M., *Physics of Semiconductor Devices*. 2'nd ed.; Wiley: 1981.

31.   S. Loth, M. Wenderoth, L. Winking, R. G. Ulbrich, S. Malzer, and G. H. Do¨hler *Phys. Rev. Lett.* **2006,** 96, 066403.

32.   Dale Kitchen, Anthony Richardella, Jian-Ming Tang, Michael E. Flatte´, Ali Yazdani. *Nature* **2006,** 442 436-439.

33.   F. Marczinowski, J. Wiebe1, J.-M. Tang, M. E. Flatté, F. Meier, M. Morgenstern, and R. Wiesendanger. *Phys. Rev. Lett.* **2007,** 99, 157202.

34.   Feenstra, R. M. *Physical Review B* **1994,** 50, (7), 4561-4570.

35.   Schlaf   R., Lang, O., Pettenkofer, C. and Jaegermann, W.   . *J. Appl. Phys.* **1999,** 85, 2732-2753

36.   Hughes, H. P., , Starnberg, H. I., *Electron Spectroscopies Applied to Low-Dimensional Structures*. Kluwer Academic Publishers: 2000.

37.   *Gmelin Handbook of Inorganic and Organometallic Chemistry*. 8th ed.; Springer-Verlag: Berlin, 1995; Vol. B7.

38.   Constant, I.; Tardif, F.; Derrien, J. *Semiconductor Science and Technology* **2000,** 15, (1), 61.

39.   A. Luican-Mayer, M. Kharitonov, Guohong Li, ChihPin Lu, I. Skachko, Alem-Mar B. Goncalves, K. Watanabe, T. Taniguchi   and E. Y. Andrei. *Physical Review Letters* **2014,** 112, 036804.